




Article

Design and Synthesis of Novel Hybrid 8-Hydroxy Quinoline-Indole Derivatives as Inhibitors of A β Self-Aggregation and Metal Chelation-Induced A β Aggregation

Suresh K. Bowroju ¹, Nirjal Mainali ² , Srinivas Ayyadevara ³, Narsimha R. Penthala ¹ , Sesha Krishnamachari ³, Samuel Kakraba ² , Robert J. Shmookler Reis ^{2,3,4} and Peter A. Crooks ^{1,*}

¹ Department of Pharmaceutical Sciences, College of Pharmacy, University of Arkansas for Medical Sciences, Little Rock, AR 72205, USA; skbowroju@uams.edu (S.K.B.); NRPenthala@uams.edu (N.R.P.)

² Bioinformatics Program, University of Arkansas at Little Rock and University of Arkansas for Medical Sciences, Little Rock, AR 72205, USA; nmainali@ualr.edu (N.M.); SKAKRABA@uams.edu (S.K.)

³ Central Arkansas Veterans Healthcare Service, University of Arkansas for Medical Sciences, Little Rock, AR 72205, USA; sesha@uams.edu (S.K.); AyyadevaraSrinivas@uams.edu (S.A.)

⁴ Department of Geriatrics, College of Medicine, University of Arkansas for Medical Sciences, Little Rock, AR 72205, USA; ReisRobertJ@uams.edu

* Correspondence: PACrooks@uams.edu

Academic Editor: Wei Li

Received: 16 July 2020; Accepted: 7 August 2020; Published: 8 August 2020



Abstract: A series of novel hybrid 8-hydroxyquinoline-indole derivatives (**7a–7e**, **12a–12b** and **18a–18h**) were synthesized and screened for inhibitory activity against self-induced and metal-ion induced A β_{1-42} aggregation as potential treatments for Alzheimer's disease (AD). In vitro studies identified the most inhibitory compounds against self-induced A β_{1-42} aggregation as **18c**, **18d** and **18f** (EC₅₀ = 1.72, 1.48 and 1.08 μ M, respectively) compared to the known anti-amyloid drug, clioquinol (**1**, EC₅₀ = 9.95 μ M). The fluorescence of thioflavin T-stained amyloid formed by A β_{1-42} aggregation in the presence of Cu²⁺ or Zn²⁺ ions was also dramatically decreased by treatment with **18c**, **18d** and **18f**. The most potent hybrid compound **18f** afforded 82.3% and 88.3% inhibition, respectively, against Cu²⁺-induced and Zn²⁺-induced A β_{1-42} aggregation. Compounds **18c**, **18d** and **18f** were shown to be effective in reducing protein aggregation in HEK-tau and SY5Y-APP_{SW} cells. Molecular docking studies with the most active compounds performed against A β_{1-42} peptide indicated that the potent inhibitory activity of **18d** and **18f** were predicted to be due to hydrogen bonding interactions, π - π stacking interactions and π -cation interactions with A β_{1-42} , which may inhibit both self-aggregation as well as metal ion binding to A β_{1-42} to favor the inhibition of A β_{1-42} aggregation.

Keywords: Alzheimer's disease; clioquinol analogues; hybrid 8-hydroxyquinoline-indole analogs; A β -aggregation; metal chelating agents

1. Introduction

Alzheimer's disease (AD) is the most debilitating age-associated neurodegenerative disorder leading to dementia, affecting millions of elderly people, and the number of patients is expected to reach 130 million worldwide by 2050 [1,2]. AD remains incurable due to the low efficacy and the very limited number of available drugs to treat this neurodegenerative disease. Salient features of AD are the accumulation of amyloid- β (A β) plaques and tangles containing hyperphosphorylated tau protein. These proteins misfold and aggregate in the brains of affected individuals as amyloid

senile plaques outside the neurons and neurofibrillary tangles (NFTs) within neurons, which are diagnostic for AD but accompanied by dyshomeostasis of biometals [3,4]. Current treatments for AD include acetylcholinesterase (AChE) inhibitors (i.e., tacrine, donepezil, rivastigmine, and galantamine), and *N*-methyl-D-aspartate (NMDA) antagonists, the only drugs approved for AD which provide a symptomatic relief strategy for mild forms of AD [5]. Unfortunately, there is currently no means to cure or even slow the progression of AD [6], spurring increased efforts to develop more effective drugs to prevent or treat AD. Due to the complexity of AD and the multitude of factors potentially involved in its progression, a strategy that uses multi-target directed ligands (MTDLs) has drawn much attention as a mainstream therapeutic approach for treatment of this disease [7–11].

The deposition of A β plays a crucial role in the pathogenesis of AD [12]. Many studies have shown that A β forms consist of several different types of aggregates, such as oligomers and fibrils [13,14]. Among these aggregates, soluble A β oligomers produce the most potent neurotoxicity and are generally regarded as the main neurotoxins in AD. Soluble A β oligomers not only lead to cognitive impairment in rodents but also induce neuronal death in primary neurons and neuronal cell cultures [15]. Soluble A β oligomers rapidly interact with neuronal cell membranes, produce free radicals, and increase the levels of intracellular reactive oxygen species (ROS) [16]. Moreover, A β oligomers induce neuronal apoptosis by regulating signaling pathways, such as glycogen synthase kinase 3 β (GSK3 β) and mitogen-activated protein kinase (MEK)/extracellular signal-regulated kinase (ERK) signaling [16]. In addition, metal ions such as Cu $^{2+}$, Zn $^{2+}$, Fe $^{2+}$, and Fe $^{3+}$ are required for neuronal activity within synapses. Due to the necessity of these metal ions, cells have a sophisticated system to maintain metal-ion homeostasis. Breakdown of these mechanisms alters the ionic balance and can result in aggregation of A β peptide into plaques, and production of reactive oxygen species induced by A β . Elevated levels of these metal ions can readily bind to A β via histidine residues H6, H13, and H14, facilitating A β aggregation [17–21] and generating reactive oxygen species (ROS) via Fenton-like reactions, which lead to oxidative stress and eventual neuronal death in AD patients [22]. Thus, clearance of A β amyloid in the brain by targeting metal ions effectively detoxifies the A β plaques, and has become a promising approach for inhibition of A β aggregation [17,20,22]. These metal ions are also implicated in the formation of hyperphosphorylated tau and tau tangles [23].

Clioquinol (CQ, **1**, Figure 1), and PBT2 (**2**, Figure 1) exhibit moderate affinity for Cu $^{2+}$ and Zn $^{2+}$ and can inhibit metal-induced A β aggregation and ROS generation in vitro [24–27]. Recently, 8-hydroxyquinoline-based multi-target-directed ligands (MTDLs), such as M30, HLA20, WBQ5187, and tacrine-8-hydroxyquinoline hybrids, have been developed for treatment of AD. These compounds significantly inhibit A β aggregation in vitro and improve cognition in vivo in mouse models [28–31]. Interestingly, the melatonin-*N*-benzylamine hybrids (**3**, Figure 1), which have an indole framework, can promote the effective development of neural stem cells into the neuronal phenotype [32,33]. The current study focuses on a series of molecules that incorporate the indole moiety and the 8-hydroxyquinoline moiety into a novel 8-hydroxyquinoline-indole hybrid structure (Figure 2; left panel). The fifth and seventh position of the 8-hydroxyquinoline moiety has also been varied by replacing the hydrogen atoms with chloro or bromo groups, followed by conjugation of these 8-hydroxyquinoline moieties to indole or 5 fluoro-, 5-chloro- or 5-methoxyindole scaffolds to improve binding affinity and metal ion selectivity. In addition, recent studies have reported that incorporating a piperazine moiety into these MTDL molecules affords significant inhibition of A β aggregation [34], which prompted us to design a second set of hybrid molecules by inserting a piperazine bridging moiety between the 8-hydroxyquinoline and indole scaffolds (Figure 2; right panel) to afford a series of novel 8-hydroxyquinoline indole ester and amide analogs as multitarget-directed drugs in AD.

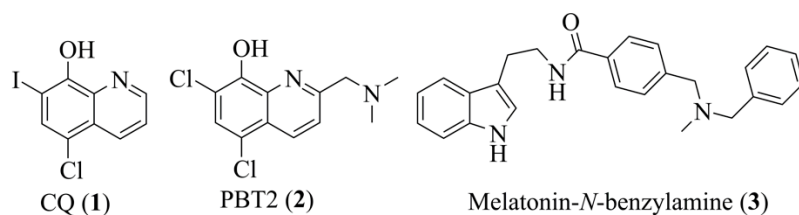


Figure 1. Chemical structures of multitarget-directed drugs clioquinol (1), PBT2 (2), and melatonin-*N*-benzylamine (3).

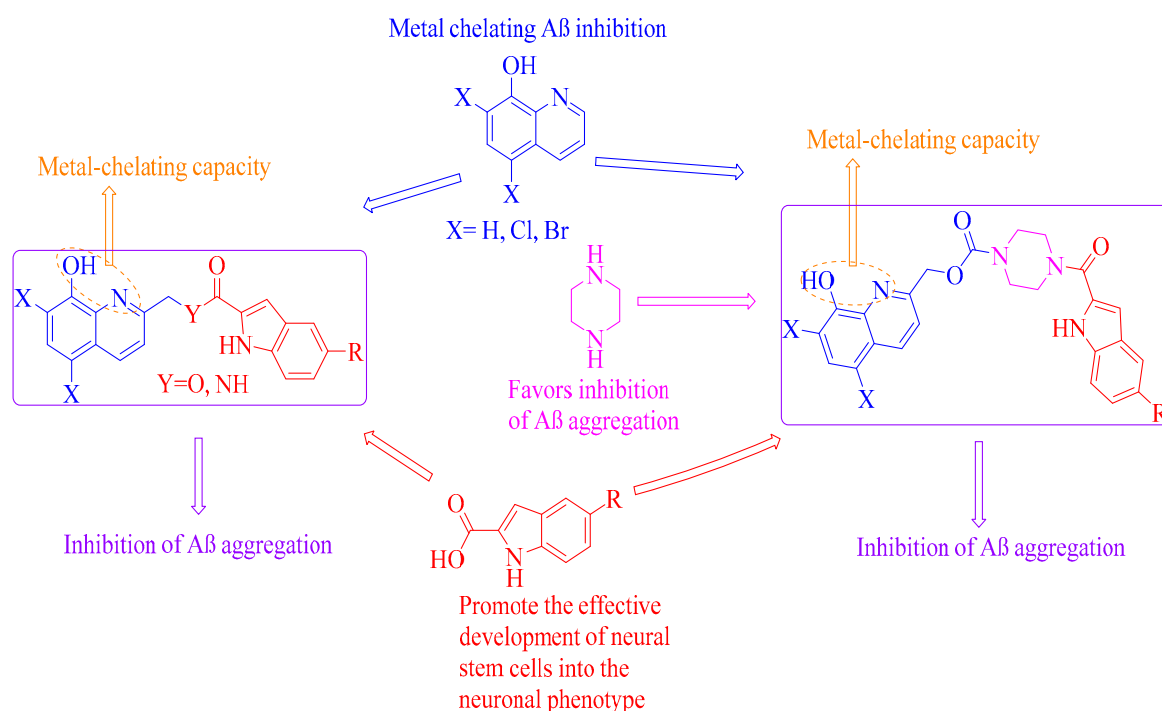


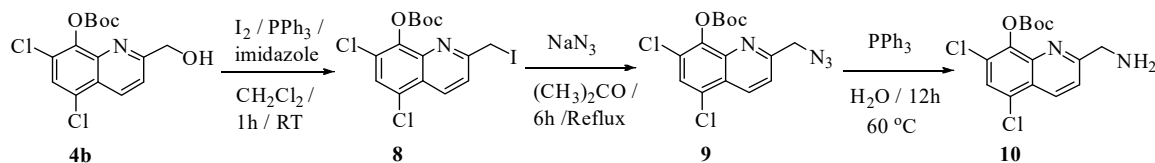
Figure 2. Design strategy for hybrid 8-hydroxyquinoline-indole ester and amide analogs with and without a piperazine-bridging moiety as multitarget-directed drugs for Alzheimer's disease (AD) therapy.

Taking into account neuronal loss, deficits in adult neurogenesis, and the formation of plaques and tangles associated with AD, the present work is focused on the identification of pharmacophores containing the 8-hydroxyquinoline moiety conjugated to an indole scaffold, in order to generate a series of hybrid 8-hydroxyquinoline indole esters and amides without (7a–7e and 12a–12b) and with a piperazine bridging moiety (18a–18h). Fifteen novel hybrid 8-hydroxyquinoline-indole analogs of this type were prepared and investigated for their inhibition of A β_{1-42} self-aggregation and metal ion-induced aggregation. Compounds which showed inhibitory activity against self-induced A β_{1-42} aggregation were also evaluated against HEK-tau and SY5Y-APP_{Sw} cells to determine their effects on cellular protein aggregation.

For the synthesis of hybrid 8-hydroxyquinoline indoles (7a–7e), we initially prepared *tert*-butyl (2-(hydroxymethyl)quinolin-8-yl) carbonates 4a and 4b utilizing literature procedures [35], and carried out EDC coupling of each compound with a variety of indole-2-carboxylic acids (5a–5c) to afford Boc-protected ester intermediates 6a–6e. Boc-deprotection of intermediates 6a–6e was carried out with trifluoroacetic acid in dichloromethane at room temperature to afford 7a–7e (Scheme 2).

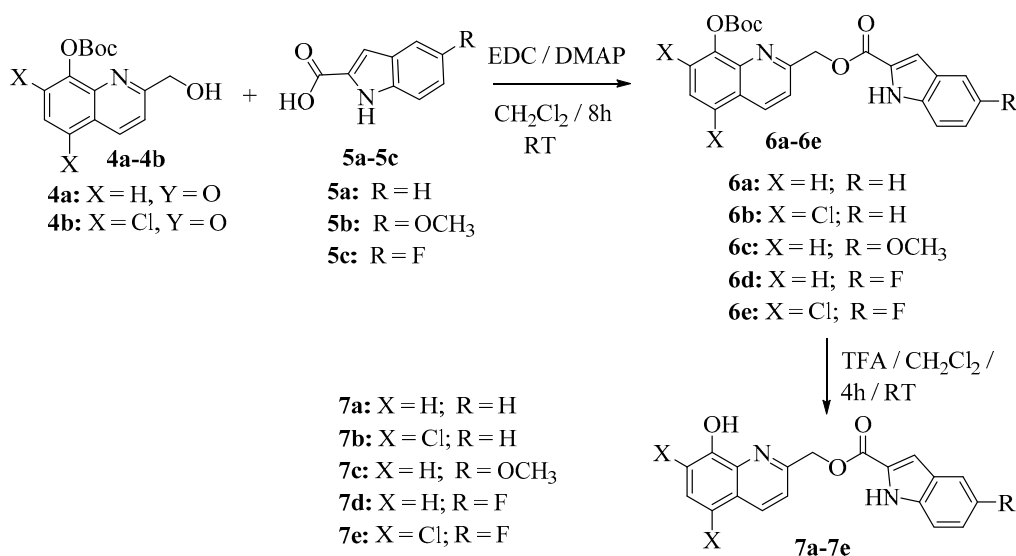
For the synthesis of hybrid *N*-((5,7-dichloro-8-hydroxyquinolin-2-yl)methyl)-1*H*-indole-2-carboxamides (12a–12b), the key intermediate 2-(aminomethyl)-5,7-dichloroquinolin-8-yl *tert*-butyl carbonate (10) was prepared by reacting intermediate 4b [35] with iodine in the presence of PPh₃ and imidazole in dichloromethane, for 1 h at room temperature, to afford iodo-intermediate 8. The product

was then reacted with sodium azide, at reflux temperature in acetone for 6 h, to afford the azido intermediate **9**. Compound **9** was then reduced to the amino compound **10** by treatment with PPh₃ in water at 60 °C for 12 h (Scheme 1).

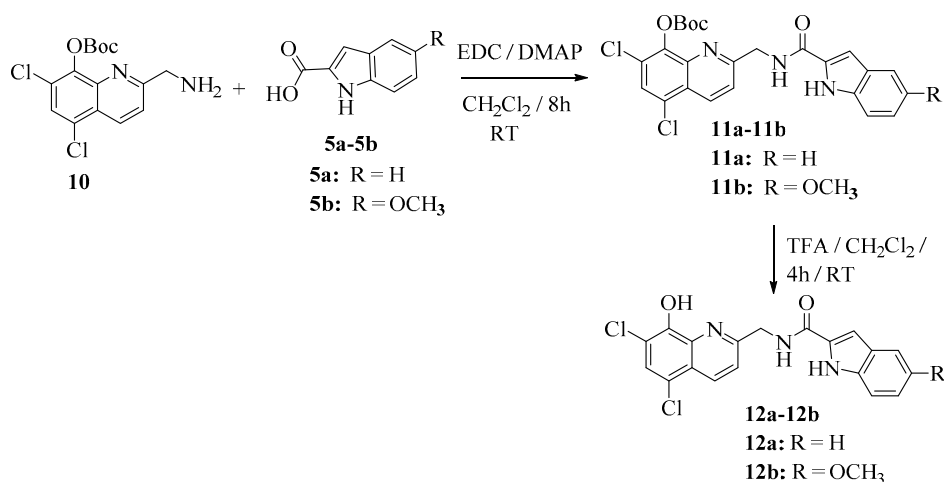


Scheme 1. Synthesis of 2-(aminomethyl)-5,7-dichloroquinolin-8-yl *tert*-butyl carbonate intermediate **10**.

Finally, EDC coupling of **10** with indole-2-carboxylic acids **5a** or **5b** afforded the Boc-protected amide intermediates **11a** and **11b**. Boc-deprotection of **11a** and **11b** was carried out with trifluoroacetic acid in dichloromethane at room temperature to afford **12a** and **12b**, respectively (Scheme 3).



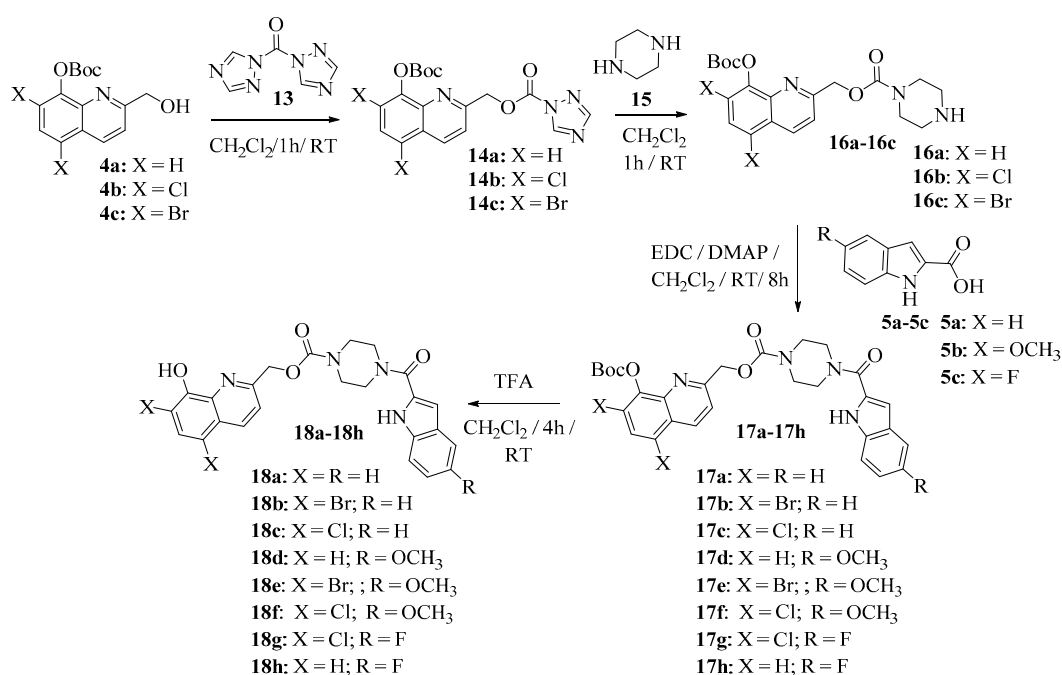
Scheme 2. Synthesis of (8-hydroxyquinolin-2-yl)methyl 1*H*-indole-2-carboxylate analogs **7a-7e**.



Scheme 3. Synthesis of *N*-((5,7-dichloro-8-hydroxyquinolin-2-yl)methyl)-1*H*-indole-2-carboxamide analogs (**12a** and **12b**).

For the synthesis of hybrid (8-hydroxyquinolin-2-yl)methyl-4-(1*H*-indole-2-carbonyl)piperazine-1-carboxylates **18a-18h**, initially we synthesized 8-(*tert*-butoxycarbonyloxyquinolin-2-yl)methyl

1*H*-1,2,4-triazole-1-carboxylate intermediates **14a–14c** by reacting *tert*-butyl (2-(hydroxymethyl)quinolin-8-yl) carbonates **4a–4c** with di-(1*H*-1,2,4-triazol-1-yl)methanone (**13**, CDT) in dichloromethane at room temperature. Compounds **14a–14c** were then each reacted with piperazine (**15**) in dichloromethane at room temperature to afford the corresponding piperazine-1-carboxylates **16a–16c**, which were subjected to EDC coupling with indole-2-carboxylic acids **5a–5c** to afford the Boc-protected intermediates **17a–17h**. Subsequent deprotection of **17a–17h** with trifluoroacetic acid in dichloromethane at room temperature over 4 h afforded the desired series of (8-hydroxyquinolin-2-yl)methyl-4-(1*H*-indole-2-carbonyl)piperazine-1-carboxylates **18a–18h** in 75–90% yields (Scheme 4). Structural confirmation of all the above intermediates and final synthetic products was obtained from ¹H-NMR, ¹³C-NMR, and HR-MS analysis (See Supplementary Materials).



Scheme 4. Synthesis of (8-hydroxyquinolin-2-yl)methyl-4-(1*H*-indole-2-carbonyl)piperazine-1-carboxylate analogs **18a–18h**.

2. Results and Discussion

The novel hybrid 8-hydroxyquinoline-indole derivatives, **7a–7e**, **12a**, **12b**, and the (8-hydroxyquinolin-2-yl)methyl-4-(1*H*-indole-2-carbonyl)piperazine-1-carboxylate analogs **18a–18h** were evaluated for inhibitory activity against self-induced A β_{1-42} aggregation at five different concentrations (0.3, 1.0, 3, 9 and 27 μ M) with 25 μ M A β_{1-42} , utilizing a thioflavin T (ThT) fluorescence assay with clioquinol, **1** as a positive control (Figure 3). In the absence of inhibitor, the self-induced A β_{1-42} aggregation ThT fluorescence was recorded as 115 arbitrary units (a.u.). The self-induced A β_{1-42} aggregation results for all the above synthetic analogs from the ThT fluorescence assay are shown in Table 1. The results indicate that analogs lacking a piperazino bridging moiety in their structure (i.e., **7a–7e** and **12a–12b**) were found to be either weak inhibitors or inactive against self-induced A β_{1-42} aggregation. Of the piperazino-containing compounds **18a–18h**, five analogs exhibited EC₅₀ values >3 μ M. 8-Hydroxyquinolin-2-yl compounds containing the piperazine bridge linked to indole (**18c**), or 5-methoxy indole (**18d** and **18f**) (EC₅₀ = 1.72, 1.48 and 1.08 μ M, respectively) were the most potent inhibitors of self-induced A β_{1-42} and were superior to both clioquinol (**1**, EC₅₀ = 9.95 μ M) and 1*H*-indole-2-carboxylic acid (**5a**, EC₅₀ > 20 μ M). The structure activity study (SAR) revealed that incorporation of the piperazino bridging moiety between a 5-methoxy indole group and a 5,7-dichloro-8-hydroxyquinoline group affords the most potent compound, **18f**, which exhibited a 10-fold improvement in inhibitory potency over **1**.

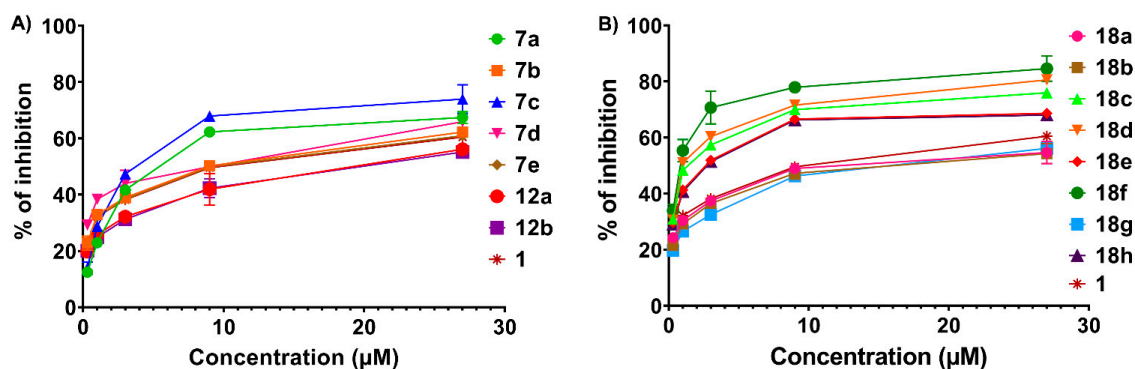


Figure 3. Dose–response curves of (A) compounds 7a–7e, 12a–12b and 1; (B) compounds 18a–18h and 1 against self-induced A β_{1-42} aggregation.

Table 1. EC₅₀ (μ M) values of compound 1, and hybrid 8-hydroxyquinoline-indole derivatives 7a–7e, 12a–12b and 18a–18h against self-induced A β_{1-42} aggregation in thioflavin T (ThT)-fluorescence assays.

Compd.	1	7a	7b	7c	7d	7e	12a	12b
A β_{1-42}	9.95	4.26	9.28	3.22	6.34	9.52	>10	>10
Compd.	18a	18b	18c	18d	18e	18f	18g	18h
A β_{1-42}	>10	>10	1.72	1.48	2.49	1.08	>10	2.58

Analogs **18c**, **18d**, and **18f**, showed potent self-induced A β_{1-42} aggregation (<2 μ M) and were selected for further investigation for inhibition of Cu²⁺- and Zn²⁺-induced A β_{1-42} aggregation. Metal ions such as Cu²⁺ and Zn²⁺ can react with A β to form A β oligomers, and then eventually to form A β amyloid plaques [8,14]. Due to their inhibitory activity against A β_{1-42} , **18c**, **18d**, and **18f** were expected to decrease metal ion-induced A β_{1-42} aggregation.

Initially, CuSO₄ or ZnCl₂ was added to A β_{1-42} peptides at room temperature and the mixture incubated with or without drugs for 24 h at 37 °C. The fluorescence intensity of A β_{1-42} peptide alone was designated as 100%. The fluorescence intensity of A β_{1-42} peptide after treatment with Cu²⁺ was 135.1% and after treatment with Zn²⁺ was 129.3% compared to A β_{1-42} alone (Figure 4A,B), indicating that both Cu²⁺ and Zn²⁺ ions significantly enhanced A β_{1-42} aggregation.

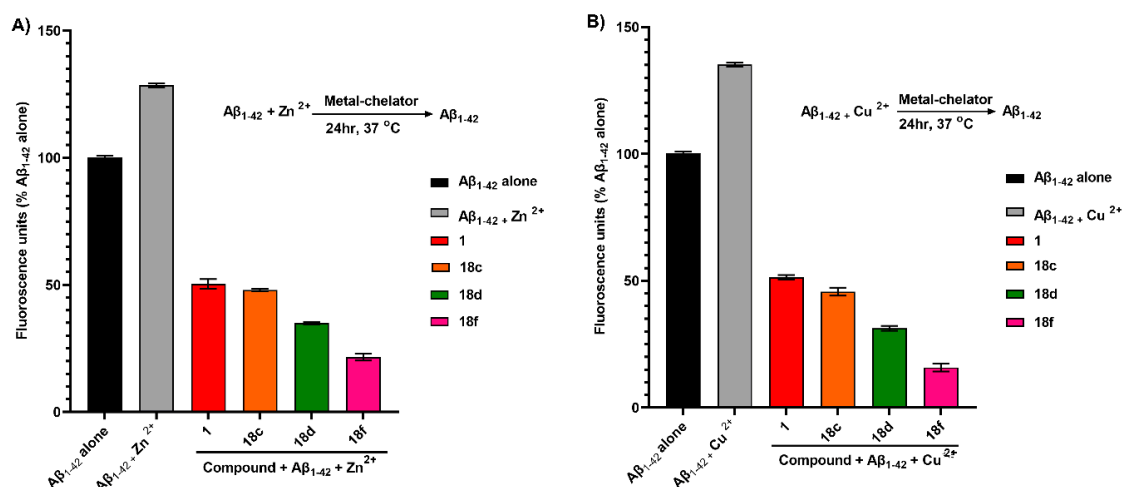


Figure 4. Effect of (A) Zn²⁺-induced and (B) Cu²⁺-induced A β_{1-42} aggregation in the presence of compound 1, **18c**, **18d**, and **18f** at 50 μ M. Data shown are presented as the mean \pm SD of three independent experiments.

In contrast, the fluorescence produced by $A\beta_{1-42}$ treated with Cu^{2+} or Zn^{2+} ions in the presence of **18c**, **18d**, and **18f** dramatically decreased (Figure 4), indicating inhibition of metal ion-induced $A\beta_{1-42}$ aggregation (i.e., **18c**, 76.6% decrease (Cu^{2+}) and 70.3% decrease (Zn^{2+}); **18d**, 66.1% decrease (Cu^{2+}) and 59.3% decrease (Zn^{2+}); **18f**, 88.3% decrease (Cu^{2+}) and 82.3% decrease (Zn^{2+}); and for comparison compound **1**, 62.5% decrease (Cu^{2+}) and 57.2% decrease (Zn^{2+})). These results show that **18f** exhibited significantly greater inhibitory activity in Cu^{2+} - and Zn^{2+} -induced $A\beta_{1-42}$ aggregation than compound **1**.

Based on the above results from self-induced $A\beta_{1-42}$ aggregation and metal-induced $A\beta_{1-42}$ aggregation studies, the most potent compounds **18f** was selected for further investigation into its ability to chelate metal ions such as Cu^{2+} , Zn^{2+} , and Fe^{2+} using UV-vis spectroscopy at wavelengths ranging from 200 to 500 nm. Compound **18f** (50 μM) was treated with 50 μM concentrations of $CuSO_4$, $ZnCl_2$, or $FeSO_4$ for 30 min in HEPES buffer at room temperature, and displayed maximum absorption wavelength shifts from 252 to 274, 269 and 255 nm in the presence of Cu^{2+} , Zn^{2+} , and Fe^{2+} , respectively (Figure 5). These wavelength shifts are indicative of the formation of **18f**- Cu^{2+} , **18f**- Zn^{2+} , and **18f**- Fe^{2+} and show that Zn^{2+} and Cu^{2+} undergo significant chelation with compound **18f**. The spectrum of **18f**- Fe^{2+} showed only a moderate increase in wavelength. Furthermore, the stoichiometry of formation of metal complexes **18f**- Cu^{2+} and **18f**- Zn^{2+} was also determined by using Job's method (Figure 6) [36]. The isosbestic points shown in Figure 6A,B at 0.6 and 0.5 imply a stoichiometry of 1.5:1 for **18f**- Cu^{2+} and 1:1 for **18f**- Zn^{2+} .

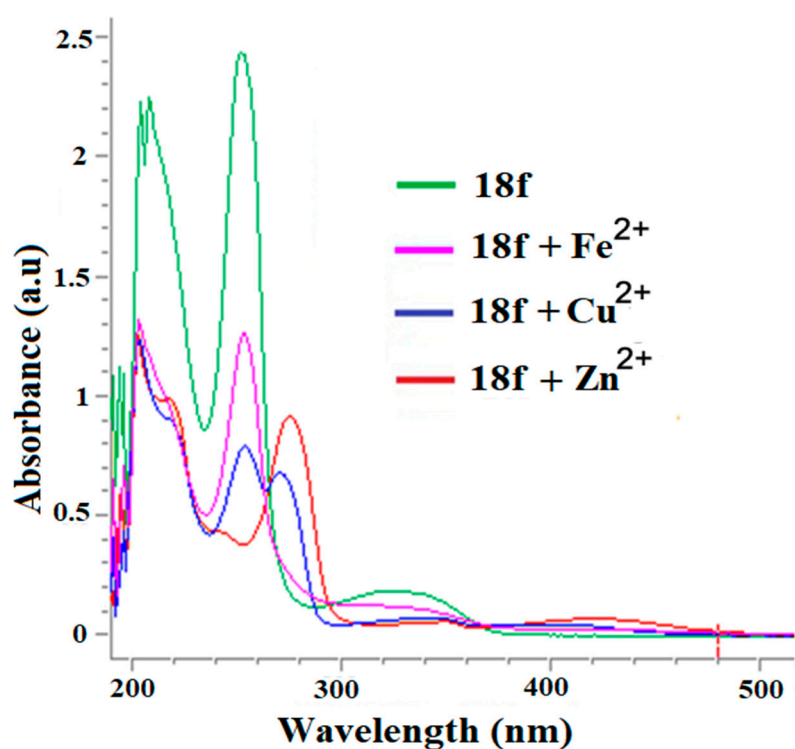


Figure 5. UV-absorbance spectra of compound **18f** (50 μM) in the presence of Cu^{2+} , Zn^{2+} , or Fe^{2+} (each at 50 μM) in buffer (20 mM HEPES, 150 mM NaCl; pH = 7.4). **18f** displayed maximum absorption wavelength shifts from 252 to 274, 269 and 255 nm in the presence of Cu^{2+} , Zn^{2+} , and Fe^{2+} , respectively.

Copper and zinc dysregulation in the brain is considered to arise as a consequence of age-associated neurodegenerative disease such as Alzheimer's disease. Zinc has also been shown to play an important role in pre- and post-synaptic responses [37]. Our drug design approach is to target dysregulation of metal homeostasis and protein aggregation. Dysregulation of metal ions is implicated in the elevated formation of reactive oxygen species and in susceptibility to oxidative stress. These metal ions were shown to interact with protein aggregation seed proteins such as tau and $A\beta_{1-42}$, increasing misfolding

and promoting protein aggregation. The 8-hydroxyquinoline compound, PBT2, has been shown to influence trans-synaptic effects of copper and zinc ions in a cell culture model and has been considered as a treatment for AD [38]. PBT2 (2) was also shown to induce amyloid degradation by inhibiting glycogen synthase kinase-3 activity via phosphorylation [38].

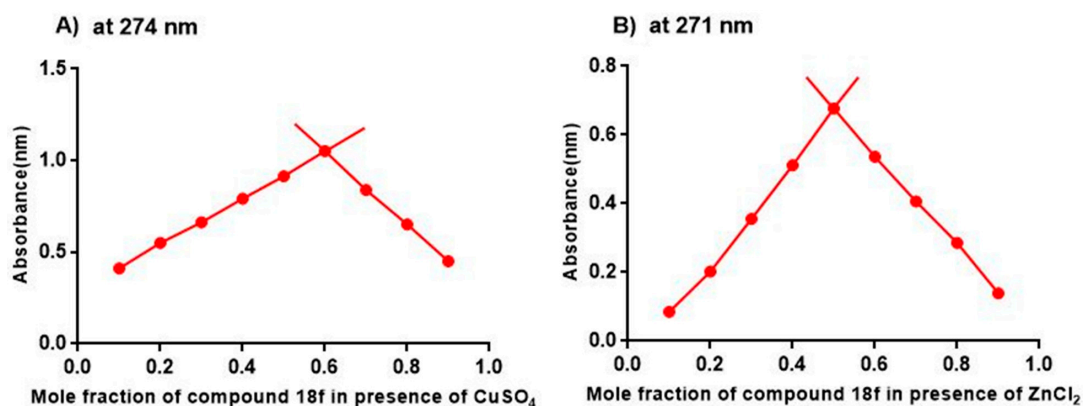


Figure 6. Determination of the stoichiometry of (A) 18f- Cu^{2+} complex and (B) the 18f- Zn^{2+} complex by Job's method [34].

In our study, we have shown that restoring metal homeostasis by treatment with hybrid 8-hydroxyquinoline-indole analogs reduces tau- and amyloid-mediated protein aggregation, and their associated neurotoxicity. Analogs 7a–7d, 18c–18f, and 18h were evaluated for their ability to reduce protein aggregation in HEK-tau cells. HEK-tau cells were exposed to the above $\text{A}\beta_{1-42}$ aggregation inhibitors and parent drug clioquinol (1) at 1 μM for 48 h at 37 °C. Cells were assessed for amyloid deposits by staining with 0.1% *w/v* thioflavin T, counterstaining nuclei with DAPI, and mean ThT fluorescence signal per nucleus was calculated over multiple fields [39]. All the analogs reduced fluorescence intensity (indicative of protein aggregation) by 26–62% ($P < 0.001$ by 2-tailed *t*-test). Among these analogs, compounds 7b–7d, 18c, and 18f were the most effective as protein aggregation inhibitors in HEK-tau cells, and were more potent than clioquinol (1) (Figure 7A,B).

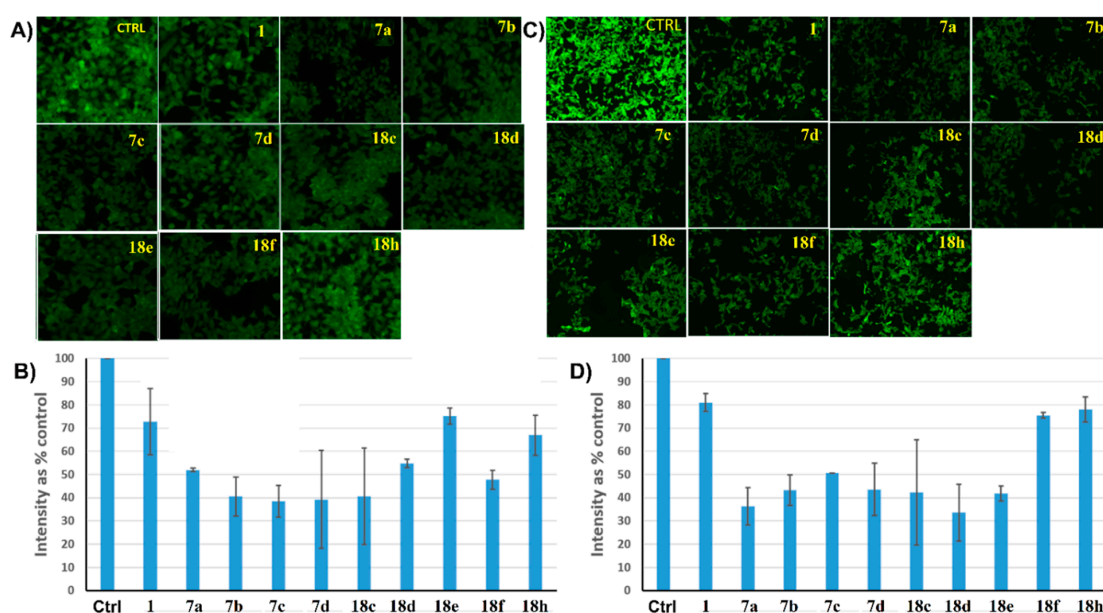


Figure 7. Amyloid-like aggregate intensity reduction by several analogs of hybrid 8-hydroxyquinoline-indoles in HEK-tau cells (A,B) and in SY5Y APP_{Sw} (neuroblastoma) cells (C,D).

In another study compounds **7a–7d**, **18c–18f**, and **18h** were also evaluated for their ability to reduce protein aggregation in SY5Y-APP_{SW} cells. SY5Y-APP_{SW} cells were exposed to the above protein aggregation inhibitors and parent compound **1** at 1 μ M for 48 h at 37 °C. Cells were assessed for amyloid deposits by staining with 0.1% *w/v* ThT, counterstaining nuclei with DAPI, and mean ThT fluorescence signal per nucleus calculated over multiple fields. All the analogs reduced fluorescence intensity (indicative of protein aggregation) by 22–67% ($P < 0.001$ by 2-tailed *t*-test). Analogs **7a** and **18d** were the most effective in SY5Y-APP_{SW} cells and were more potent than the parent compound, clioquinol (**1**) (Figure 7C,D). Thioflavin-T fluorescence assays for in vitro amyloid aggregation and cell culture models of amyloid aggregation overlap but are not identical. This is due to the fact that thioflavin in cell-culture stains not just amyloid aggregates but also other amyloid-like fibrillar structures. Another important difference is that in vitro aggregation is assessed after 24 h, whereas aggregation in cell culture is assessed after 48 h.

The binding interactions of the active compounds **18d** and **18f** were also investigated utilizing a crystal structure of the target A β _{1–42} peptide (PDB code: 1IYT) [40] employing Schrodinger Maestro 11.4 software (Figure 8) [41]. For analogue **18d**, the quinoline ester carbonyl group of this hybrid molecule is involved in a hydrogen bonding interaction with Lys16 at a distance of 3.12 Å units and the 8-hydroxyquinoline moiety is involved in a π – π stacking interaction with residue Phe20; this is similar to that observed with the deoxyvasicinone-donepezil hybrid molecule binding region on A β _{1–42} reported in the literature [41]. In addition, the quinolone and indole ring systems of compound **18d** are involved in π –cation interactions with Lys16. With the potent analog **18f**, the hydroxyl group of the 8-hydroxyquinoline moiety is involved in a hydrogen bonding interaction with the His13 residue at 2.17 Å units, and the 8-hydroxyquinoline moiety of **18f** is also involved in a π – π stacking interaction with Phe20, similar to the binding mode of compound **18d**. In addition, the quinoline ring system of **18f** is involved in a π –cation interaction with Lys16. These docking results indicate that the effective inhibition of both self-induced and metal ion-induced A β _{1–42} aggregation by **18d** and **18f** may be due to hydrogen bonding interactions, π – π stacking interactions, and π –cation interactions of these molecules. Of particular interest is the interaction the most potent compound **18f** with the His13 residue on the A β _{1–42} peptide. His13 has been implicated in the binding of metal ions with A β _{1–42} (17–21); thus, **18f** may compete with metal ions for this binding site on A β _{1–42}, thereby inhibiting metal ion induction of A β _{1–42} aggregation.

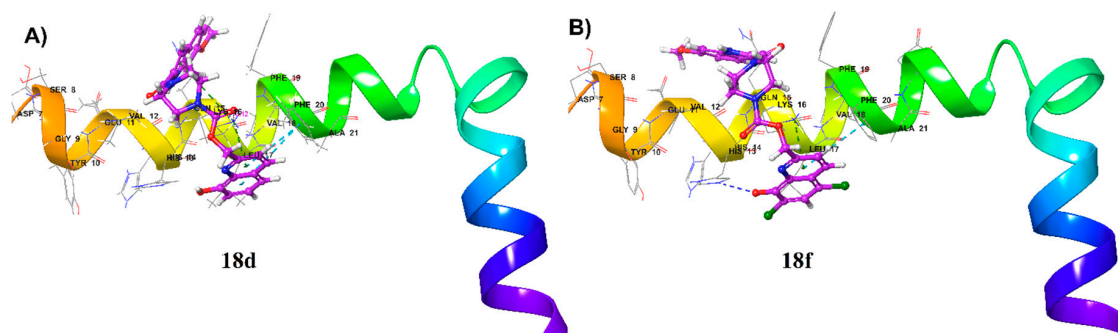


Figure 8. Proposed binding modes of (A) compound **18d** and (B) **18f** with A β _{1–42} peptide.

In summary, a series of hybrid 8-hydroxyquinoline-indole derivatives **7a–7e**, **12a–12b**, and **18a–18h** have been synthesized and evaluated as inhibitors of A β _{1–42} self-aggregation and metal chelation-induced aggregation, and have also been evaluated against HEK-tau and SY5Y-APP_{SW} cells to determine their effect on cellular protein aggregation. In vitro studies showed that hybrid 8-hydroxyquinoline-indole analogs lacking the piperazine bridging unit (i.e., compounds **7a–7e** and **12a–12b**) exhibited poor-to-moderate inhibitory activities against A β _{1–42} peptide self-aggregation. However, the majority of the hybrid 8-hydroxyquinoline-indole compounds incorporating the piperazine bridge unit (i.e., **18c–18f**, and **18h**) were potent inhibitors against A β _{1–42} self-aggregation.

Analogue **18f** was the most potent inhibitor of A β_{1-42} aggregation in both self-induced and metal chelation-induced assays, and in protein aggregation assays in HEK-tau cells. Compound **18f** afforded 82.3% and 88.3% inhibition against Cu²⁺-induced and Zn²⁺-induced A β_{1-42} aggregation assays, and was also shown to be a chelator of Cu²⁺, Zn²⁺, and Fe²⁺ ions in physiological buffer solutions. Molecular docking studies with **18f** showed that this molecule has the potential to interact with the His13 residue on A β_{1-42} peptide, which suggests that its potent anti-aggregation properties may also be due in part to its ability to competitively inhibit the binding of metal ions that interact with this site to induce A β_{1-42} aggregation. Thus, the present study has identified **18f**, an analog that incorporates a piperazine bridging group between a 5-methoxyindole moiety and a 5,7-dichloro-8-hydroxyquinoline moiety, as the most potent A β_{1-42} aggregation inhibitor; this analog exhibited a 10-fold improvement in inhibitory potency over clioquinol (**1**) as an inhibitor of A β_{1-42} self-aggregation. We consider **18f** to be a lead compound worthy of further structural optimization and preclinical development as a treatment for AD.

3. Experimental Section

3.1. Chemistry

All reagents, solvents, and chemicals utilized in the synthesis of the hybrid 8-hydroxyquinoline-indole analogs were purchased from Oakwood Chemicals Fisher Scientific and Adooq Bioscience. ¹H and ¹³C-NMR spectra were recorded on a Varian 400 MHz spectrometer equipped with a Linux workstation running on vNMRj software. Spectral analyses were carried out in CDCl₃ or DMSO-*d*₆ for both ¹H and ¹³C spectra. Chemical shifts were measured in δ parts per million (*ppm*) and coupling constants (*J*) were measured in hertz (Hz). High-resolution mass spectra (HR-MS) were recorded on an Agilent 6545 ESI/APCI TOF MS. Thin-layer chromatography (TLC) was carried out on pre-coated silica gel glass plates (F254 Merck).

3.2. Experimental Procedure for the Synthesis of Hybrid 8-Hydroxyquinoline-Indole Analogs

Synthesis of (8-hydroxyquinolin-2-yl)methyl-1H-indole-2-carboxylate hybrid analogs **7a–7e**

To a stirred solution of an appropriate indole-2-carboxylic acid (**5a–5c**) (0.15 mmol) in dry dichloromethane (5 mL) under an argon atmosphere at 0 °C was added 1-ethyl-3-(3-dimethylamino propyl)carbodiimide (EDCI, 0.181 mmol), and the mixture allowed to stir for 15 min. A catalytic amount of 4-dimethylaminopyridine (DMAP, 0.045 mmol) was then added, followed by addition of an appropriate *tert*-butyl (2-(hydroxymethyl)quinolin-8-yl) carbonate (**4a–4b**) (0.151 mmol) in dry dichloromethane (3 mL) at 0 °C. The resulting mixture was stirred for 8 h at room temperature. After completion of the reaction (monitored by TLC), the reaction mixture was washed with water (10 mL), and the dichloromethane layer separated, dried over anhydrous sodium sulfate, filtered, concentrated, and purified by silica gel column chromatography using 2–5% methanolic dichloromethane as eluent to afford the corresponding Boc-protected 8-hydroxyquinoline-indole derivatives (**6a–6e**).

The above Boc-protected 8-hydroxyquinoline-indole derivatives (**6a–6e**) were each dissolved in a mixture of DCM (10 mL) and TFA (1.0 mL) and stirred for 6 h until the Boc-deprotection was completed. A saturated NaHCO₃ solution (20 mL) was then added and the resulting mixture was extracted with dichloromethane. The organic layer was separated and washed with water, followed by brine solution, dried over anhydrous Na₂SO₄, and concentrated to afford the appropriate hybrid 8-hydroxyquinoline indole derivatives (**7a–7e**).

(8-Hydroxyquinolin-2-yl)methyl-1H-indole-2-carboxylate (**7a**): ¹H-NMR (400 MHz, DMSO-*d*₆): δ 12.00 (s, 1H), 9.67 (s, 1H), 8.38 (d, *J* = 8.4 Hz, 1H), 7.76–6.3 (m, 2H), 7.52–7.37 (m, 3H), 7.35–7.22 (m, 2H), 7.13–7.07 (m, 2H), 5.64 (s, 2H) *ppm*. ¹³C-NMR (100 MHz, DMSO-*d*₆): δ 161.44, 154.70, 153.40, 138.08, 138.01, 137.56, 128.57, 127.99, 127.16, 127.14, 125.34, 122.59, 120.73, 120.35, 118.15, 113.06, 112.19, 108.99, 67.50 *ppm*. HR-MS (ESI) *m/z* calcd for C₁₉H₁₄N₂O₃ (M + H)⁺ 319.1075, found 319.1076.

(5,7-Dichloro-8-hydroxyquinolin-2-yl)methyl-1H-indole-2-carboxylate (**7b**): $^1\text{H-NMR}$ (400 MHz, $\text{DMSO-}d_6$): δ 12.02 (s, 1H), 10.67 (s, 1H), 8.58 (d, $J = 8.8$ Hz, 1H), 7.91 (d, $J = 8.8$ Hz, 1H), 7.84 (s, 1H), 7.7 (d, $J = 8.0$ Hz, 1H), 7.49 (d, $J = 8.8$ Hz, 1H), 7.33 (s, 1H), 7.29 (t, $J = 7.6$ Hz, 1H), 7.10 (t, $J = 7.6$ Hz, 1H), 5.70 (s, 2H) ppm. $^{13}\text{C-NMR}$ (100 MHz, $\text{DMSO-}d_6$): δ 161.35, 156.98, 149.23, 138.68, 138.05, 134.50, 128.27, 127.15, 126.97, 125.42, 124.61, 122.62, 121.61, 120.77, 119.58, 116.56, 113.06, 109.14, 67.02 ppm. HR-MS (ESI) m/z calcd for $\text{C}_{19}\text{H}_{12}\text{Cl}_2\text{N}_2\text{O}_3$ ($\text{M} + \text{H}$) $^+$ 387.0291, found 387.0296.

(8-Hydroxyquinolin-2-yl)methyl-5-methoxy-1H-indole-2-carboxylate (**7c**): $^1\text{H-NMR}$ (400 MHz, $\text{DMSO-}d_6$): δ 11.87 (s, 1H), 9.67 (s, 1H), 8.38 (d, $J = 8.4$ Hz, 1H), 7.70 (d, $J = 8.4$ Hz, 1H), 7.46–7.35 (m, 3H), 7.2 (s, 1H), 7.12 (d, $J = 2.8$ Hz, 2H), 6.95 (d, $J = 8.8$ Hz, 1H), 5.63 (s, 2H), 3.76 (s, 3H) ppm. $^{13}\text{C-NMR}$ (100 MHz, $\text{DMSO-}d_6$): δ 161.36, 154.76, 154.44, 153.40, 138.08, 137.55, 133.40, 128.57, 127.98, 127.49, 127.30, 120.33, 118.15, 117.03, 113.98, 112.18, 108.55, 102.39, 67.40, 55.65 ppm. HR-MS (ESI) m/z calcd for $\text{C}_{20}\text{H}_{16}\text{N}_2\text{O}_4$ ($\text{M} + \text{H}$) $^+$ 349.1174, found 349.1178.

(8-Hydroxyquinolin-2-yl)methyl-5-fluoro-1H-indole-2-carboxylate (**7d**): $^1\text{H-NMR}$ (400 MHz, $\text{DMSO-}d_6$): δ 12.13 (s, 1H), 9.67 (s, 1H), 8.38 (d, $J = 8.4$ Hz, 1H), 7.71 (d, $J = 8.4$ Hz, 1H), 7.50–7.40 (m, 4H), 7.28 (s, 1H), 7.19–7.11 (m, 2H), 5.64 (s, 2H) ppm. $^{13}\text{C-NMR}$ (100 MHz, $\text{DMSO-}d_6$): δ 161.17, 158.86, 156.54, 154.58, 153.41, 138.09, 137.57, 134.75, 128.80, 128.58, 128.01, 127.24, 127.13, 120.37, 118.15, 114.49, 114.39, 114.20, 112.20, 108.88, 108.83, 106.66, 106.43, 67.62 ppm. HR-MS (ESI) m/z calcd for $\text{C}_{19}\text{H}_{13}\text{FN}_2\text{O}_3$ ($\text{M} + \text{H}$) $^+$ 337.0969, found 337.0978.

(5,7-Dichloro-8-hydroxyquinolin-2-yl)methyl-5-fluoro-1H-indole-2-carboxylate (**7e**): $^1\text{H-NMR}$ (400 MHz, $\text{DMSO-}d_6$): δ 12.14 (s, 1H), 10.64 (s, 1H), 8.57 (d, $J = 8.8$ Hz, 1H), 7.91 (d, $J = 8.8$ Hz, 1H), 7.83 (s, 1H), 7.50 (m, 2H), 7.30 (d, $J = 2.0$ Hz, 1H), 7.16 (td, $J = 9.2, 2.4$ Hz, 1H), 5.67 (s, 2H) ppm; $^{13}\text{C-NMR}$ (100 MHz, $\text{DMSO-}d_6$): δ 161.09, 158.87, 156.83, 156.54, 149.20, 138.66, 134.78, 134.47, 128.62, 128.26, 127.21, 127.11, 124.59, 121.59, 119.57, 116.55, 114.54, 114.49, 114.39, 114.27, 109.01, 108.95, 106.67, 106.44, 67.13 ppm. HR-MS (ESI) m/z calcd for $\text{C}_{19}\text{H}_{11}\text{Cl}_2\text{FN}_2\text{O}_3$ ($\text{M} + \text{H}$) $^+$ 405.0187, found 405.0199.

Synthesis of *tert*-butyl (5,7-dichloro-2-(iodomethyl)quinolin-8-yl) carbonate (**8**):

To a stirred solution of *tert*-butyl-(5,7-dichloro-2-(hydroxymethyl)quinolin-8-yl) carbonate **4b** (1 mmol) was added triphenyl phosphine (1.2 mmol), imidazole (1.3 mmol) in dichloromethane, and iodine (1.2 mmol) at room temperature. The resulting reaction mixture was stirred for 1 h. After completion of the reaction, aqueous sodium dithionite solution was added and the resulting mixture extracted with dichloromethane, the separated organic layer was dried over Na_2SO_4 and concentrated under reduced pressure. The crude product was purified by column chromatography (silica gel, 10% ethyl acetate in hexanes) to afford compound **8**.

$^1\text{H-NMR}$ (400 MHz, CDCl_3): δ 8.42 (d, $J = 8.4$ Hz, 1H), 7.62 (s, 1H), 7.61 (d, $J = 8.8$ Hz, 1H), 4.61 (s, 2H), 1.60 (s, 9H) ppm. $^{13}\text{C-NMR}$ (101 MHz, CDCl_3): δ 160.22, 150.41, 142.71, 141.54, 134.27, 128.76, 127.40, 127.34, 124.70, 122.56, 84.43, 27.67, 5.41 ppm.

Synthesis of 2-(azidomethyl)-5,7-dichloroquinolin-8-yl *tert*-butyl carbonate (**9**):

To a stirred solution of *tert*-butyl-(5,7-dichloro-2-(iodomethyl)quinolin-8-yl) carbonate **8** (1 mmol) in acetone was added sodium azide (3 mmol). The resulting mixture was stirred at reflux temperature for 6 h. After completion of the reaction, the reaction mixture was cooled to room temperature then solvent was evaporated. Water was added to the crude mass and mixture extracted with dichloromethane, the separated organic layer dried over Na_2SO_4 and concentrated under reduced pressure. The crude product was purified by column chromatography (silica gel, 1% methanol in dichloromethane) to afford compound **9**.

$^1\text{H-NMR}$ (CDCl_3 , 400 MHz): δ 8.49 (d, $J = 8.8$ Hz, 1H), 8.00 (s, 1H), 7.60 (d, $J = 8.4$ Hz, 1H), 4.64 (s, 2H), 1.59 (s, 9H) ppm. $^{13}\text{C-NMR}$ (CDCl_3 , 101 MHz): δ $^{13}\text{C-NMR}$ (101 MHz, CDCl_3): δ 158.07, 150.27, 144.91, 141.76, 137.04, 133.13, 126.94, 121.31, 118.93, 117.11, 84.41, 77.30, 76.98, 76.67, 55.60, 27.61 ppm.

Synthesis of 2-(aminomethyl)-5,7-dichloroquinolin-8-yl *tert*-butyl carbonate (**10**):

To a stirred solution of 2-(azidomethyl)-5,7-dichloroquinolin-8-yl *tert*-butyl carbonate **9** (1 mmol) in THF/H₂O (3 mL, 9:1) was added PPh₃ (1.2 mmol) at room temperature. The resulting reaction mixture was stirred at 60 °C for 12 h. After completion of reaction, the reaction mixture was concentrated under vacuum and 1 M aqueous HCl added to the residue. The mixture was stirred for 30 min, then the mixture was filtered to get aqueous phase. The aqueous phase was basified to pH 10 with NaHCO₃ and extracted with dichloromethane. The combined organic layer was washed with brine, dried over anhydrous Na₂SO₄, and the solution was evaporated under vacuum to afford target compound **10**.

¹H-NMR (400 MHz, CDCl₃): δ 8.41 (d, *J* = 8.7 Hz, 1H), 7.63 (s, 1H), 7.39 (d, *J* = 8.7 Hz, 1H), 4.89 (s, 2H), 1.58 (s, 9H) *ppm*. ¹³C-NMR (101 MHz, CDCl₃): δ 161.16, 150.50, 142.37, 140.93, 134.02, 129.02, 127.64, 127.17, 125.30, 119.75, 84.65, 77.29, 77.17, 76.97, 76.65, 64.14, 27.58 *ppm*.

Synthesis of *N*-((8-hydroxyquinolin-2-yl)methyl)-1*H*-indole-2-carboxamide hybrid analogs **12a** and **12b**:

To a stirred solution of indole-2-carboxylic acid **5a** or **5b** (0.15 mmol) in dry dichloromethane (5 mL) under an argon atmosphere at 0 °C was added EDCI (0.181 mmol) and the mixture allowed to stir for 15 min. A catalytic amount of DMAP (0.045 mmol) was then added followed by addition of 2-(aminomethyl)-5,7-dichloroquinolin-8-yl *tert*-butyl carbonate (**10**) (0.151 mmol) in dry dichloromethane (3 mL) at 0 °C, and the resulting mixture was stirred for 8 h at room temperature. After completion of the reaction (monitored by TLC), the reaction mixture was washed with water (10 mL), and the dichloromethane layer separated, dried over anhydrous sodium sulfate, filtered, concentrated, and purified by silica gel column chromatography, using 2–5% methanolic dichloromethane as eluent, to afford the corresponding Boc-protected 8-hydroxyquinoline-indole derivatives **11a** or **11b** as a solid. Products were obtained in 56–74% yield.

The above Boc-protected 8-hydroxyquinoline-indole derivatives **11a** and **11b** were each dissolved in a mixture of DCM (10 mL) and trifluoroacetic acid (TFA, 1.0 mL) and the resulting mixture stirred for 6 h until the Boc-deprotection was completed. A saturated NaHCO₃ solution (20 mL) was then added and the resulting mixture extracted with dichloromethane. The organic layer was separated and washed with water, followed by brine solution, dried over anhydrous Na₂SO₄, and concentrated to afford the appropriate hybrid 8-hydroxyquinoline indole derivatives **12a** and **12b**.

N-((5,7-Dichloro-8-hydroxyquinolin-2-yl)methyl)-1*H*-indole-2-carboxamide (**12a**): ¹H-NMR (400 MHz, DMSO-*d*₆): δ 12.01 (s, 1H), 10.71 (s, 1H), 10.07 (s, 1H), 8.52(d, *J* = 8.4 Hz, 1H), 8.07 (s, 1H), 7.93 (d, *J* = 8.8 Hz, 1H), 7.70 (d, *J* = 8.0 Hz, 1H), 7.49 (d, *J* = 8.0 Hz, 1H), 7.33 (s, 1H), 7.28 (t, *J* = 7.6 Hz, 1H), 7.12 (t, *J* = 7.6 Hz, 1H), 5.71 (s, 2H) *ppm*; ¹³C-NMR (100 MHz, DMSO-*d*₆): δ 161.34, 156.89, 151.03, 138.59, 138.05, 137.00, 133.70, 127.14, 126.97, 126.25, 125.41, 122.61, 122.08, 120.77, 113.06, 109.39, 109.14, 106.03, 66.91 *ppm*. HR-MS (ESI) *m/z* calcd for C₁₉H₁₃Cl₂N₃O₂ (M + H)⁺ 386.0379, found 386.0382.

N-((5,7-Dichloro-8-hydroxyquinolin-2-yl)methyl)-5-methoxy-1*H*-indole-2-carboxamide (**12b**): ¹H-NMR (400 MHz, DMSO-*d*₆): δ 11.87 (s, 1H), 10.64 (s, 1H), 10.02 (s, 1H), 8.56 (d, *J* = 8.8 Hz, 1H), 7.87 (d, *J* = 8.8 Hz, 1H), 7.8 (s, 1H), 7.35 (d, *J* = 9.2 Hz, 1H), 7.2–7.19 (m, 1H), 7.11 (d, *J* = 2.4 Hz, 1H), 6.94 (dd, *J* = 8.8, 2.4 Hz, 1H), 5.67 (s, 2H), 3.74 (s, 3H) *ppm*; ¹³C-NMR (100 MHz, DMSO-*d*₆): δ 161.26, 157.04, 154.46, 149.21, 138.68, 134.49, 133.43, 128.26, 127.47, 127.10, 124.60, 121.59, 119.58, 117.13, 116.55, 113.98, 108.68, 102.37, 66.93, 55.65 *ppm*. HR-MS (ESI) *m/z* calcd for C₂₀H₁₅Cl₂N₃O₃ (M + H)⁺ 416.0485, found 416.0492.

Synthesis of (8-((*tert*-butoxycarbonyl)oxy)quinolin-2-yl)methyl-1*H*-1,2,4-triazole-1-carboxylates **14a–14c**:

To a stirred solution of an appropriate *tert*-butyl (2-(hydroxymethyl)quinolin-8-yl) carbonate (**4a–4c**) (1 mmol) in dichloromethane was added carbonylditriazole (2 mmol) at room temperature. The reaction mixture was stirred for 30 min. After completion of the reaction, water was added and the resulting mixture was extracted with dichloromethane, the separated organic layer dried over Na₂SO₄ and concentrated under reduced pressure to afford triazole intermediates **14a–14c**.

(8-((*tert*-Butoxycarbonyl)oxy)quinolin-2-yl)methyl-1*H*-1,2,4-triazole-1-carboxylate (**14a**):

¹H-NMR (400 MHz, CDCl₃): δ 8.88 (s, 1H), 8.27 (d, *J* = 8.5 Hz, 1H), 8.11 (s, 1H), 7.74 (dd, *J* = 6.6, 3.0 Hz, 1H), 7.63 (d, *J* = 8.5 Hz, 1H), 7.58–7.50 (m, 2H), 5.77 (s, 2H), 1.59 (s, 9H) ppm. ¹³C-NMR (101 MHz, CDCl₃): δ 153.83, 153.68, 151.83, 147.28, 145.79, 140.60, 137.46, 128.89, 126.90, 125.61, 121.67, 119.87, 83.70, 71.17, 27.62 ppm.

(8-((*tert*-Butoxycarbonyl)oxy)-5,7-dichloroquinolin-2-yl)methyl-1*H*-1,2,4-triazole-1-carboxylate (**14b**):

¹H-NMR (400 MHz, CDCl₃): δ 8.89 (s, 1H), 8.59 (d, *J* = 8.8 Hz, 1H), 8.11 (s, 1H), 7.71 (d, *J* = 8.4 Hz, 2H), 5.77 (s, 2H), 1.57 (s, 9H) ppm. ¹³C-NMR (101 MHz, CDCl₃): δ 155.61, 153.90, 150.35, 145.84, 142.78, 141.72, 134.77, 128.95, 127.86, 125.42, 120.29, 84.57, 70.38, 27.54 ppm.

(8-((*tert*-Butoxycarbonyl)oxy)-5,7-dibromoquinolin-2-yl)methyl-1*H*-1,2,4-triazole-1-carboxylate (**14c**):

¹H-NMR (400 MHz, CDCl₃): δ 8.89 (s, 1H), 8.54 (d, *J* = 8.7 Hz, 1H), 8.08 (d, *J* = 30.9 Hz, 2H), 7.71 (d, *J* = 8.8 Hz, 1H), 5.78 (s, 2H), 1.58 (s, 9H) ppm. ¹³C-NMR (101 MHz, CDCl₃): δ 155.53, 153.88, 150.16, 147.26, 145.86, 144.92, 141.67, 137.30, 133.51, 127.12, 120.74, 118.92, 117.35, 84.52, 70.23, 27.55 ppm.

Synthesis of hybrid (8-((*tert*-butoxycarbonyl)oxy)quinolin-2-yl)methylpiperazine-1-carboxylates **16a–16c**:

An appropriate triazole intermediate (**14a–14c**) (1 mmol) was dissolved in dichloromethane (2 mL) and treated with piperazine (**15**) (1.0 mmol) at room temperature for 1 h. Completion of the reaction was monitored by TLC. Water (2 mL) was then added and the resulting mixture was extracted with dichloromethane (2 × 3 mL), the organic layer separated, dried over anhydrous Na₂SO₄ and concentrated to afford the appropriate Boc-protected product (**16a–16c**). The crude product was purified by column chromatography (silica gel, 2% methanol in dichloromethane) to afford the desired product (**16a–16c**).

(8-((*tert*-Butoxycarbonyl)oxy)quinolin-2-yl)methyl-piperazine-1-carboxylate (**16a**): ¹H-NMR (400 MHz, DMSO-*d*₆): δ 8.33 (d, *J* = 8.4 Hz, 1H), 7.52 (d, *J* = 8.4 Hz, 1H), 7.45–7.35 (m, 2H), 7.10 (dd, *J* = 7.2, 1.2 Hz, 1H), 5.33 (s, 2H), 3.37 (m, 4H), 2.72–2.61 (m, 4H), 1.58 (s, 9H) ppm; ¹³C-NMR (101 MHz, DMSO-*d*₆): δ 155.59, 154.75, 153.35, 153.22, 137.99, 137.42, 128.43, 127.80, 119.91, 118.08, 112.07, 67.84, 45.81, 27.52 ppm.

(8-((*tert*-Butoxycarbonyl)oxy)-5,7-dichloro-8-hydroxyquinolin-2-yl)methyl-piperazine-1-carboxylate (**16b**): ¹H-NMR (400 MHz, CDCl₃): δ 8.39 (d, *J* = 8.4 Hz, 1H), 7.52 (d, *J* = 8.8 Hz, 1H), 7.48 (s, 1H), 5.37 (s, 2H), 3.59 (m, 4H), 2.88 (br-s, 4H), 1.57 (s, 9H) ppm; ¹³C-NMR (101 MHz, CDCl₃): δ 156.66, 153.64, 154.82, 147.78, 137.93, 134.32, 128.07, 124.18, 120.40, 120.31, 115.78, 67.22, 53.42, 45.49, 27.52 ppm.

(8-((*tert*-Butoxycarbonyl)oxy)-5,7-dibromo-8-hydroxyquinolin-2-yl)methyl-piperazine-1-carboxylate (**16c**): ¹H-NMR (400 MHz, DMSO-*d*₆): δ 8.40 (d, *J* = 8.8 Hz, 1H), 7.97 (s, 1H), 7.68 (d, *J* = 8.8 Hz, 1H), 5.38 (s, 2H), 3.46 (m, 4H), 2.80 (br-s, 4H), 1.58 (s, 9H) ppm; ¹³C-NMR (101 MHz, DMSO-*d*₆): δ 156.92, 154.60, 153.55, 153.13, 139.44, 136.71, 133.63, 126.37, 121.45, 106.98, 106.32, 67.49, 45.01, 44.33, 27.51 ppm.

Synthesis of (8-hydroxyquinolin-2-yl)methyl-4-(1*H*-indole-2-carbonyl)piperazine-1-carboxylate hybrid derivatives (**18a–18h**):

To the stirred solution of an appropriate indole-2-carboxylic acid (**5a–5c**) (0.15 mmol) in dry dichloromethane (5 mL) under an argon atmosphere at 0 °C was added EDCI (0.181 mmol), and the mixture allowed to stir for 15 min. A catalytic amount of DMAP (0.045 mmol) was then added, followed by addition of an appropriate (8-((*tert*-butoxycarbonyloxy)-quinolin-2-yl)methyl piperazine-1-carboxylate (**16a–16c**) (0.151 mmol) in dry dichloromethane (3 mL) at 0 °C. The resulting mixture was stirred for 8 h at room temperature. After completion of the reaction (monitoring by TLC), the reaction mixture was washed with water (10 mL) and

the dichloromethane layer separated, dried over anhydrous sodium sulfate, filtered, and concentrated. The crude material was purified by silica gel column chromatography, using 2–5% methanolic dichloromethane as eluent, to afford the corresponding (8-((*tert*-butoxycarbonyloxy)quinolin-2-yl)methyl-4-(1*H*-indole-2-carbonyl)piperazine-1-carboxylate hybrid derivatives (**17a–17h**), which was dissolved in a mixture of DCM (10 mL) and TFA (1.0 mL) and stirred for 6 h until Boc-deprotection was completed. Saturated NaHCO₃ solution (20 mL) was then added to the resulting mixture which was extracted with dichloromethane. The organic layer was separated and washed with water, followed by brine solution, dried over anhydrous Na₂SO₄ and concentrated to afford the corresponding (8-hydroxyquinolin-2-yl)methyl-4-(1*H*-indole-2-carbonyl)piperazine-1-carboxylate hybrid derivative (**18a–18h**).

(8-Hydroxyquinolin-2-yl)methyl-4-(1*H*-indole-2-carbonyl)piperazine-1-carboxylate (**18a**): ¹H-NMR (400 MHz, CDCl₃): δ 9.67 (s, 1H), 8.19 (d, *J* = 8.4 Hz, 1H), 7.65 (d, *J* = 8.0 Hz, 1H), 7.52–7.42 (m, 3H), 7.35–7.2 (m, 2H), 7.20–7.12 (m, 2H), 6.78 (s, 1H), 5.45 (s, 2H), 3.96 (s, 4H), 3.70 (s, 4H) ppm; ¹³C-NMR (100 MHz, CDCl₃): δ 162.82, 154.94, 154.26, 151.88, 137.07, 127.85, 124.64, 121.87, 120.66, 120.06, 117.73, 111.71, 110.44, 105.49, 68.12, 43.74 ppm. HR-MS (ESI) *m/z* calcd for C₂₄H₂₂N₄O₄ (M + H)⁺ 431.1708, found 431.1712.

(5,7-Dibromo-8-hydroxyquinolin-2-yl)methyl-4-(1*H*-indole-2-carbonyl)piperazine-1-carboxylate (**18b**): ¹H-NMR (400 MHz, CDCl₃): δ 9.50 (s, 1H), 8.44 (d, *J* = 8.8 Hz, 1H), 7.86 (s, 1H), 7.61 (dd, *J* = 15.2, 8.4 Hz, 2H), 7.41 (d, *J* = 8.0 Hz, 1H), 7.28 (t, *J* = 7.6 Hz, 1H), 7.13 (t, *J* = 7.6 Hz, 1H), 6.76 (s, 1H), 5.46 (s, 2H), 3.96 (s, 4H), 3.68 (s, 4H) ppm; ¹³C-NMR (100 MHz, CDCl₃): δ 162.75, 156.36, 154.69, 149.35, 137.77, 137.09, 135.75, 133.78, 128.62, 127.32, 125.92, 124.69, 121.91, 121.05, 120.73, 111.78, 110.07, 105.50, 104.33, 67.38, 44.03 ppm. HR-MS (ESI) *m/z* calcd for C₂₄H₂₀Br₂N₄O₄ (M + H)⁺ 588.9879, found 588.9885.

(5,7-Dichloro-8-hydroxyquinolin-2-yl)methyl-4-(1*H*-indole-2-carbonyl)piperazine-1-carboxylate (**18c**): ¹H-NMR (400 MHz, CDCl₃): δ 10.08 (s, 1H), 8.41 (d, *J* = 8.8 Hz, 1H), 7.63 (d, *J* = 7.6 Hz, 1H), 7.56 (d, *J* = 8.4 Hz, 1H), 7.5 (s, 1H), 7.42 (d, *J* = 7.6 Hz, 1H), 7.27 (d, *J* = 7.6 Hz, 1H), 7.13 (t, *J* = 7.2 Hz, 1H), 6.76 (s, 1H), 5.45 (s, 2H), 3.99 (s, 4H), 3.7 (s, 4H) ppm. ¹³C-NMR (100 MHz, CDCl₃): δ 162.98, 156.40, 154.75, 147.29, 137.69, 135.95, 134.42, 128.61, 128.14, 127.22, 124.54, 124.13, 121.84, 120.68, 120.61, 120.45, 115.68, 111.89, 105.52, 67.48, 43.82 ppm. HR-MS (ESI) *m/z* calcd for C₂₄H₂₀Cl₂N₄O₄ (M + H)⁺ 499.0925, found 499.0929.

(8-Hydroxyquinolin-2-yl)methyl-4-(5-methoxy-1*H*-indole-2-carbonyl)piperazine-1-carboxylate (**18d**): ¹H-NMR (400 MHz, DMSO-*d*₆): δ 11.46 (s, 1H), 9.64 (s, 1H), 8.34 (d, *J* = 8.4 Hz, 1H), 7.58 (d, *J* = 8.4 Hz, 1H), 7.45–7.38 (m, 2H), 7.33 (d, *J* = 8.8 Hz, 1H), 7.12 (d, *J* = 6.8 Hz, 1H), 7.07 (s, 1H), 6.86 (dd, *J* = 8.8, 2.4 Hz, 1H), 6.75 (s, 1H), 5.38 (s, 2H), 3.81 (br-s, 4H), 3.75 (s, 3H), 3.63 (br-s, 2H), 3.56 (br-s, 2H) ppm; ¹³C-NMR (100 MHz, DMSO-*d*₆): δ 162.65, 155.37, 154.78, 154.18, 153.37, 138.03, 137.43, 131.66, 130.37, 128.50, 127.83, 127.52, 120.01, 118.13, 114.89, 113.36, 112.13, 104.51, 102.31, 68.09, 55.66, 44.04 ppm. HR-MS (ESI) *m/z* calcd for C₂₅H₂₄N₄O₅ (M + H)⁺ 461.1811, found 461.1813.

(5,7-Dibromo-8-hydroxyquinolin-2-yl)methyl-4-(5-methoxy-1*H*-indole-2-carbonyl)piperazine-1-carboxylate (**18e**): ¹H-NMR (400 MHz, DMSO-*d*₆): δ 11.46 (s, 1H), 8.48 (d, *J* = 8.8 Hz, 1H), 8.05 (s, 1H), 7.8 (d, *J* = 8.8 Hz, 1H), 7.33 (d, *J* = 9.2 Hz, 1H), 7.07 (d, *J* = 2.0 Hz, 1H), 6.85 (dd, *J* = 8.8, 2.4 Hz, 1H), 6.75 (s, 1H), 5.45 (s, 2H), 3.821 (s, 4H), 3.75 (s, 3H), 3.65 (br-s, 4H) ppm. ¹³C-NMR (100 MHz, DMSO-*d*₆): δ 162.66, 157.61, 154.62, 154.18, 151.04, 138.57, 136.89, 133.57, 131.66, 130.35, 127.51, 126.16, 121.75, 114.90, 113.36, 109.33, 105.98, 104.52, 102.30, 67.54, 55.67 ppm. HR-MS (ESI) *m/z* calcd for C₂₅H₂₂Br₂N₄O₅ (M + H)⁺ 618.9998, found 619.0000.

(5,7-Dichloro-8-hydroxyquinolin-2-yl)methyl-4-(5-methoxy-1*H*-indole-2-carbonyl)piperazine-1-carboxylate (**18f**): ¹H-NMR (400 MHz, DMSO-*d*₆): δ 11.46 (s, 1H), 8.54 (d, *J* = 8.8 Hz, 1H), 7.80 (s, 1H), 7.78 (d, *J* = 8.8 Hz, 1H), 7.33 (d, *J* = 8.8 Hz, 1H), 7.06 (d, *J* = 2.4 Hz, 1H), 6.85 (dd, *J* = 8.8, 2.4 Hz, 1H), 6.74 (s, 1H), 5.44 (s, 2H), 4.04 (s, 2H), 3.82 (s, 2H), 3.75 (s, 3H), 3.66 (s, 2H), 3.54 (s, 2H) ppm; ¹³C-NMR (100 MHz, DMSO-*d*₆): δ 162.66, 162.61, 157.66, 154.61, 154.17, 149.09, 138.58, 134.32, 131.65, 131.50, 130.32, 130.18,

128.09, 127.49, 127.45, 124.49, 121.23, 119.58, 116.43, 114.88, 113.34, 113.29, 104.49, 104.45, 102.25, 67.63, 44.09, 40.54, 40.33, 40.12, 39.91, 39.70, 39.49, 39.28 ppm. HR-MS (ESI) m/z calcd for $C_{25}H_{22}Cl_2N_4O_5$ (M + H)⁺ 529.1026, found 529.1031.

(5,7-Dichloro-8-hydroxyquinolin-2-yl)methyl-4-(5-fluoro-1H-indole-2-carbonyl)piperazine-1-carboxylate (**18g**): ¹H-NMR (400 MHz, DMSO-*d*₆): δ 11.73 (s, 1H), 8.52 (d, *J* = 8.8 Hz, 1H), 7.80 (s, 1H), 7.77 (d, *J* = 8.8 Hz, 1H), 7.43 (dd, *J* = 8.8, 4.8 Hz, 1H), 7.37 (d, *J* = 10.0 Hz, 1H), 7.05 (t, *J* = 9.2 Hz, 1H), 6.83 (s, 1H), 5.44 (s, 2H), 3.82 (s, 4H), 3.66 (br-s, 2H), 3.55 (br-s, 2H) ppm. ¹³C-NMR (100 MHz, DMSO-*d*₆): δ 162.35, 158.72, 157.60, 156.40, 154.62, 149.28, 138.66, 134.30, 133.13, 131.83, 128.11, 127.33, 127.22, 124.50, 121.22, 119.42, 116.47, 113.77, 113.67, 112.57, 112.31, 106.04, 105.81, 104.72, 104.67, 67.66, 43.92 ppm. HR-MS (ESI) m/z calcd for $C_{24}H_{19}Cl_2FN_4O_4$ (M + H)⁺ 517.0829, found 517.0833.

(5,7-Dibromo-8-hydroxyquinolin-2-yl)methyl-4-(5-fluoro-1H-indole-2-carbonyl)piperazine-1-carboxylate (**18h**): ¹H-NMR (400 MHz, DMSO-*d*₆): δ 11.72 (s, 1H), 9.65 (s, 1H), 8.35 (d, *J* = 8.4 Hz, 1H), 7.58 (d, *J* = 8.4 Hz, 1H), 7.45–7.35 (m, 4H), 7.12–7.03 (m, 2H), 6.83 (d, *J* = 1.6 Hz, 1H), 5.38 (s, 2H), 3.81 (br-s, 4H), 3.63 (br-s, 2H), 3.54 (br-s, 2H) ppm. ¹³C-NMR (101 MHz, DMSO-*d*₆): δ 162.33, 158.71, 156.39, 155.35, 154.78, 153.35, 138.01, 137.44, 133.12, 131.83, 128.50, 127.84, 127.33, 127.22, 120.01, 118.14, 113.77, 113.67, 112.57, 112.31, 112.14, 106.05, 105.82, 104.74, 104.69, 68.09, 44.0. HR-MS (ESI) m/z calcd for $C_{24}H_{21}FN_4O_4$ (M + H)⁺ 449.1621, found 449.1616.

3.3. Methodology for the In Vitro Self-Induced Aβ_{1–42} Aggregation Assay

The thioflavin T (ThT)-fluorescence assay was used to measure the inhibition of Aβ aggregation [42]. Aβ_{1–42} (Adooq Bioscience, CA, USA) was pretreated with 1 mL of hexafluoroisopropanol (HFIP) to afford a stock solution, which was aliquoted into small samples. The solvent was evaporated at room temperature, and samples were stored at –80 °C. For Aβ_{1–42} aggregation inhibition experiments, phosphate buffer (pH 7.4) was added to the Aβ stock solution to afford a 50 μM concentration before use. A mixture of the Aβ_{1–42} peptide (10 μL, 25 μM final concentration) with or without the test compound (10 μL; 0.3, 1.0, 3, 9, and 27 μM) was incubated at 37 °C for 48 h. Blanks using phosphate buffer (pH 7.4) instead of Aβ, with or without test compound, were also assessed. Then 50 mM glycine-NaOH buffer (pH 8.0) containing ThT (5 μM) was added to 20 μL of the sample to afford a final volume of 200 μL. The fluorescence intensities were recorded (excitation, 450 nm; emission, 485 nm). The fluorescence intensities were background corrected to the no enzyme control and 100% of intensity reflected no inhibition of aggregation. To obtain the normalized amyloid aggregation inhibition relative to the control group, the amyloid aggregation/cell values were further divided by the total amyloid fluorescence of the control group. Using GraphPad Prism, the amyloid aggregation values (relative to control group) were entered along the corresponding concentrations for the triplicates and then a log transformation was obtained. Using the dose–response simulation module in GraphPad Prism, nonlinear regression fit (curve) was then generated for each small molecule with various concentrations used. Curves were then compared to determine if they were statistically different, by performing the best-fit values of selected unshared parameters between data sets and extra sum-of-squares F test, allowing for selection of the simpler model unless the *P* value was less than 0.05. The logEC₅₀ output parameter was then selected to obtain the EC₅₀ for each of the dose–response curves for the small molecules.

3.4. Methodology for the In Vitro Metal-Induced Aβ_{1–42} Aggregation Assay

For the inhibition of copper- and zinc-mediated Aβ_{1–42} aggregation, 20 μM HEPES (pH 6.6) in 150 μM NaCl was added to the Aβ_{1–42} stock solution to afford a 25 μM solution. Mixtures of the peptide (10 μL, 25 μM final concentration) with or without Cu²⁺ or Zn²⁺ (10 μL, 25 μM final concentration) and the test compound (10 μL, 50 μM final concentration) were incubated at 37 °C for 24 h. Then 50 mM glycine-NaOH buffer (pH 8.0) containing ThT (5 μM) was added to 20 μL of the sample and diluted to afford a final volume of 200 μL. Fluorescence intensities of the solutions were recorded

(excitation, 450 nm; emission, 485 nm). The percentage of aggregation was calculated by the expression $(1 - IF_i/IF_c) \times 100$, in which IF_i and IF_c are the fluorescence intensities obtained for $A\beta$ in the presence and absence of inhibitors, respectively.

3.5. Methodology for the Metal-Chelation Study

The chelating studies were performed with a UV-vis spectrophotometer. The absorption spectra of test compound (50 μ M, final concentration) alone or in the presence of $CuSO_4$, $FeSO_4$, or $ZnCl_2$ (50 μ M, final concentration) in buffer (20 mM HEPES, 150 mM NaCl, pH 7.4) were incubated for 30 min and then recorded at room temperature, respectively. For the stoichiometry of the test compound- Cu^{2+} complex or the test compound- Zn^{2+} complex, a fixed amount of test compound (50 μ M) was mixed with increasing amounts of copper ion or Zn ion (0–100 μ M), and the UV-vis difference spectra were analyzed to determine the ratio of ligand/metal ion in the complex.

3.6. Methodology for In Vitro HEK-Tau and SY5Y-APP_{Sw} Cell Aggregation Assays

Human Embryonic Kidney cells that overexpress tau protein (HEK-tau) cells or SY5Y neuroblastoma cells that express a familial-AD mutant of amyloid precursor protein (SY5Y-APP_{Sw} cells) were each seeded in 96-well plates at 8000 cells per well. After 24 h, cells were supplemented with test compound at 1 μ M after diluting with medium. Vehicle only control was also included for each experiment. The cells were cultured for an additional 48 h at 37 °C. Both the cell lines were able to reach approximately 80% confluency in 48 h. Cells were assessed for amyloid deposits by staining with 0.1% *w/v* ThT, counterstaining nuclei with DAPI, and calculating mean ThT fluorescence signal per nucleus over multiple fields.

3.7. Methodology for Molecular Docking

Molecular docking was performed using Schrodinger software Maestro 11.4 suite. The ligands were prepared using the LigPrep module. The protein crystal structure PDB ID: 1IYT was downloaded from the RCSB Protein Data Bank (<https://www.rcsb.org/>). The downloaded protein crystal structure was prepared in Protein Preparation Wizard wherein the missing hydrogens were added and bond orders assigned. A grid for docking the ligand was generated with the centroid of the co-crystallized ligand from PDB ID: 1IYT as the center of the grid with no constraints. The prepared ligands **18d** and **18f** were docked into this grid using Glide module. Molecular docking was performed at XP precision and results were analyzed in the Maestro visualizer.

Supplementary Materials: The following are available online.

Author Contributions: S.K.B.: Design, Synthesis and In vitro self-induced and metal-Induced $A\beta_{1-42}$ aggregation assay; N.M. and S.K. (Sesha Krishnamachari): In vitro HEK-Tau and SY5Y-APP_{Sw} cell culture experiments; S.A.: Design of screening the drugs against $A\beta_{1-42}$ aggregation and cell culture experiments; N.R.P.: Molecular docking studies; S.K. (Samuel Kakraba): Calculations of in vitro self-induced and metal-Induced $A\beta_{1-42}$ aggregation assay results; R.J.S.R.: Supervision and design of overall biological experiments; P.A.C.: Supervision and design of overall project; S.K.B. and N.R.P.: Manuscript preparation with additional inputs from P.A.C. All authors have read and agreed to the published version of the manuscript.

Funding: We are grateful for research support from the National Institutes of Health, NIA grant P01 AG012411 (S. Griffin, P.I.) and from the U.S. Dept. of Veteran Affairs, Merit Award BX001655 (R. J. Shmookler Reis, P.I.); also a Senior Research Career Scientist Award BX004851 to R.J.S.R.; and an Arkansas Research Alliance Scholar award to P.A.C.

Conflicts of Interest: The authors declare no conflicts of interest.

References

1. Förstl, H.; Kurz, A. Clinical features of Alzheimer's disease. *Eur. Arch. Psy. Clin. Neurosci.* **1999**, *249*, 288–290. [[CrossRef](#)] [[PubMed](#)]
2. Torre, J.D.; Aliev, G.; Perry, G. Drug Therapy in Alzheimer's Disease. *N. Engl. J. Med.* **2004**, *351*, 1911–1913.
3. Querfurth, H.W.; LaFerla, F.M. Alzheimer's disease. *N. Engl. J. Med.* **2010**, *362*, 329–344. [[CrossRef](#)]

4. Walsh, D.M.; Selkoe, D.J. Deciphering the molecular basis of memory failure in Alzheimer's disease. *Neuron* **2004**, *44*, 181–193. [[CrossRef](#)]
5. Munoz-Torrero, D. Acetylcholinesterase inhibitors as disease-modifying therapies for Alzheimer's disease. *Curr. Med. Chem.* **2008**, *15*, 2433–2455. [[CrossRef](#)]
6. Young, A.B. Four decades of neurodegenerative disease research: How far we have come! *J. Neurosci.* **2009**, *29*, 12722–12728. [[CrossRef](#)]
7. Spangenberg, E.E.; Green, K.N. Inflammation in Alzheimer's disease: Lessons learned from microglia-depletion models. *Brain Behav. Immun.* **2017**, *61*, 1–11. [[CrossRef](#)]
8. Deora, G.S.; Kantham, S.; Chan, S.; Dighe, S.N.; Veliyath, S.K.; McColl, G.; Parat, M.O.; McGeary, R.P.; Ross, B.P. Multifunctional Analogs of Kynurenic Acid for the Treatment of Alzheimer's Disease: Synthesis, Pharmacology, and Molecular Modeling Studies. *ACS Chem. Neurosci.* **2017**, *8*, 2667–2675. [[CrossRef](#)] [[PubMed](#)]
9. Hiremathad, A.; Keri, R.S.; Esteves, A.R.; Cardoso, S.M.; Chaves, S.; Santos, M.A. Novel Tacrine-Hydroxyphenylbenzimidazole hybrids as potential multitarget drug candidates for Alzheimer's disease. *Eur. J. Med. Chem.* **2018**, *148*, 255–267. [[CrossRef](#)] [[PubMed](#)]
10. Kumar, B.; Dwivedi, A.R.; Sarkar, B.; Gupta, S.K.; Krishnamurthy, S.; Mantha, A.K.; Parkash, J.; Kumar, V. 4,6-Diphenylpyrimidine Derivatives as Dual Inhibitors of Monoamine Oxidase and Acetylcholinesterase for the Treatment of Alzheimer's Disease. *ACS Chem. Neurosci.* **2019**, *10*, 252–265. [[CrossRef](#)]
11. Li, X.; Wang, H.; Xu, Y.; Liu, W.; Gong, Q.; Wang, W.; Qiu, X.; Zhu, J.; Mao, F.; Zhang, H.; et al. Novel Vilazodone-Tacrine Hybrids as Potential Multitarget-Directed Ligands for the Treatment of Alzheimer's Disease Accompanied with Depression: Design, Synthesis, and Biological Evaluation. *ACS Chem. Neurosci.* **2017**, *8*, 2708–2721. [[CrossRef](#)] [[PubMed](#)]
12. Sevigny, J.; Chiao, P.; Bussiere, T.; Weinreb, P.H.; Williams, L.; Maier, M.; Dunstan, R.; Salloway, S.; Chen, T.; Ling, Y.; et al. The antibody aducanumab reduces Abeta plaques in Alzheimer's disease. *Nature* **2016**, *537*, 50–56. [[CrossRef](#)] [[PubMed](#)]
13. Mohamed, T.; Shakeri, A.; Rao, P.P. Amyloid cascade in Alzheimer's disease: Recent advances in medicinal chemistry. *Eur. J. Med. Chem.* **2016**, *113*, 258–272. [[CrossRef](#)] [[PubMed](#)]
14. Viola, K.L.; Klein, W.L. Amyloid- β oligomers in Alzheimer's disease pathogenesis, treatment, and diagnosis. *Acta Neuropathol.* **2015**, *129*, 183–206. [[CrossRef](#)]
15. Chang, L.; Cui, W.; Yang, Y.; Xu, S.; Zhou, W.; Fu, H.; Hu, S.; Mak, S.; Hu, J.; Wang, Q.; et al. Protection against β -amyloid-induced synaptic and memory impairments via altering β -amyloid assembly by bis(heptyl)-cognitin. *Sci. Rep.* **2015**, *5*, 10256. [[CrossRef](#)]
16. Zhao, L.N.; Long, H.; Mu, Y.; Chew, L.Y. The toxicity of amyloid β oligomers. *Int. J. Mol. Sci.* **2012**, *13*, 7303–7327. [[CrossRef](#)]
17. Barnham, K.J.; Bush, A.I. Metals in Alzheimer's and Parkinson's diseases. *Curr. Opin. Chem. Biol.* **2008**, *12*, 222–228. [[CrossRef](#)]
18. Himes, R.A.; Park, G.Y.; Siluvai, G.S.; Blackburn, N.J.; Karlin, K.D. Structural studies of copper(I) complexes of amyloid- β peptide fragments: Formation of two-coordinate bis(histidine) complexes. *Angew. Chem. Int. Ed. Engl.* **2008**, *47*, 9084–9087. [[CrossRef](#)]
19. Hou, L.; Zagorski, M.G. NMR reveals anomalous copper(II) binding to the amyloid Abeta peptide of Alzheimer's disease. *J. Am. Chem. Soc.* **2006**, *128*, 9260–9261. [[CrossRef](#)]
20. Duce, J.A.; Bush, A.I. Biological metals and Alzheimer's disease: Implications for therapeutics and diagnostics. *Prog. Neurobiol.* **2010**, *92*, 1–18. [[CrossRef](#)]
21. Kepp, K.P. Bioinorganic Chemistry of Alzheimer's Disease. *Chem. Rev.* **2012**, *112*, 5193–5239. [[CrossRef](#)] [[PubMed](#)]
22. Savelieff, M.G.; DeToma, A.S.; Derrick, J.S.; Lim, M.H. The ongoing search for small molecules to study metal-associated amyloid- β species in Alzheimer's disease. *Acc. Chem. Res.* **2014**, *47*, 2475–2482. [[CrossRef](#)]
23. Kim, A.C.; Lim, S.; Kim, Y.K. Metal Ion Effects on A β and Tau Aggregation. *Int. J. Mol. Sci.* **2018**, *19*, 128. [[CrossRef](#)] [[PubMed](#)]

24. Ritchie, C.W.; Bush, A.I.; Mackinnon, A.; Macfarlane, S.; Mastwyk, M.; MacGregor, L.; Kiers, L.; Cherny, R.; Li, Q.X.; Tammer, A.; et al. Metal-protein attenuation with iodochlorhydroxyquin (clioquinol) targeting Abeta amyloid deposition and toxicity in Alzheimer disease: A pilot phase 2 clinical trial. *Arch. Neurol.* **2003**, *60*, 1685–1691. [[CrossRef](#)] [[PubMed](#)]
25. Cherny, R.A.; Atwood, C.S.; Xilinas, M.E.; Gray, D.N.; Jones, W.D.; McLean, C.A.; Barnham, K.J.; Volitakis, I.; Fraser, F.W.; Kim, Y.; et al. Treatment with a copper-zinc chelator markedly and rapidly inhibits β -amyloid accumulation in Alzheimer's disease transgenic mice. *Neuron* **2001**, *30*, 665–676. [[CrossRef](#)]
26. Adlard, P.A.; Cherny, R.A.; Finkelstein, D.I.; Gautier, E.; Robb, E.; Cortes, M.; Volitakis, I.; Liu, X.; Smith, J.P.; Perez, K.; et al. Rapid restoration of cognition in Alzheimer's transgenic mice with 8-hydroxy quinoline analogs is associated with decreased interstitial Abeta. *Neuron* **2008**, *59*, 43–55. [[CrossRef](#)]
27. Faux, N.G.; Ritchie, C.W.; Gunn, A.; Rembach, A.; Tsatsanis, A.; Bedo, J.; Harrison, J.; Lannfelt, L.; Blennow, K.; Zetterberg, H.; et al. PBT2 rapidly improves cognition in Alzheimer's Disease: Additional phase II analyses. *J. Alzheimers Dis.* **2010**, *20*, 509–516. [[CrossRef](#)]
28. Fernandez-Bachiller, M.I.; Perez, C.; Gonzalez-Munoz, G.C.; Conde, S.; Lopez, M.G.; Villarroya, M.; Garcia, A.G.; Rodriguez-Franco, M.I. Novel tacrine-8-hydroxyquinoline hybrids as multifunctional agents for the treatment of Alzheimer's disease, with neuroprotective, cholinergic, antioxidant, and copper-complexing properties. *J. Med. Chem.* **2010**, *53*, 4927–4937. [[CrossRef](#)]
29. Zheng, H.; Gal, S.; Weiner, L.M.; Bar-Am, O.; Warshawsky, A.; Fridkin, M.; Youdim, M.B. Novel multifunctional neuroprotective iron chelator-monoamine oxidase inhibitor drugs for neurodegenerative diseases: In vitro studies on antioxidant activity, prevention of lipid peroxide formation and monoamine oxidase inhibition. *J. Neurochem.* **2005**, *95*, 68–78. [[CrossRef](#)]
30. Zheng, H.; Youdim, M.B.; Fridkin, M. Site-activated multifunctional chelator with acetylcholinesterase and neuroprotective-neurorestorative moieties for Alzheimer's therapy. *J. Med. Chem.* **2009**, *52*, 4095–4098. [[CrossRef](#)]
31. Wang, Z.; Wang, Y.; Wang, B.; Li, W.; Huang, L.; Li, X. Design, Synthesis, and Evaluation of Orally Available Clioquinol-Moracin M Hybrids as Multitarget-Directed Ligands for Cognitive Improvement in a Rat Model of Neurodegeneration in Alzheimer's Disease. *J. Med. Chem.* **2015**, *58*, 8616–8637. [[CrossRef](#)] [[PubMed](#)]
32. López-Iglesias, B.; Pérez, C.; Morales-García, J.A.; Alonso-Gil, S.; Pérez-Castillo, A.; Romero, A.; López, M.G.; Villarroya, M.; Conde, S.; Rodríguez-Franco, M.I. New Melatonin-*N,N*-Dibenzyl(*N*-methyl)amine Hybrids: Potent Neurogenic Agents with Antioxidant, Cholinergic, and Neuroprotective Properties as Innovative Drugs for Alzheimer's Disease. *J. Med. Chem.* **2014**, *57*, 3773–3785. [[CrossRef](#)] [[PubMed](#)]
33. Ramirez-Rodriguez, G.; Klempin, F.; Babu, H.; Benitez-King, G.; Kempermann, G. Melatonin modulates cell survival of new neurons in the hippocampus of adult mice. *Neuropsychopharmacology* **2009**, *34*, 2180–2191. [[CrossRef](#)]
34. Yang, X.; Cai, P.; Liu, Q.; Wu, J.; Yin, Y.; Wang, X.; Kong, L. Novel 8-hydroxyquinoline derivatives targeting β -amyloid aggregation, metal chelation and oxidative stress against Alzheimer's disease. *Bioorg. Med. Chem.* **2018**, *26*, 3191–3201. [[CrossRef](#)] [[PubMed](#)]
35. Liang, S.H.; Southon, A.G.; Fraser, B.H.; Krause-Heuer, A.M.; Zhang, B.; Shoup, T.M.; Lewis, R.; Volitakis, I.; Han, Y.; Greguric, I.; et al. Novel Fluorinated 8-Hydroxyquinoline Based Metal Ionophores for Exploring the Metal Hypothesis of Alzheimer's Disease. *ACS Med. Chem. Lett.* **2015**, *6*, 1025–1029. [[CrossRef](#)] [[PubMed](#)]
36. Gil, V.M.S.; Oliveira, N.C. On the use of the method of continuous variations. *J. Chem. Educ.* **1990**, *67*, 473. [[CrossRef](#)]
37. Sensi, S.L.; Paoletti, P.; Koh, J.Y.; Aizenman, E.; Bush, A.I.; Hershfinkel, M. The neurophysiology and pathology of brain zinc. *J. Neurosci.* **2011**, *31*, 16076–16085. [[CrossRef](#)]
38. Crouch, P.J.; Savva, M.S.; Hung, L.W.; Donnelly, P.S.; Mot, A.I.; Parker, S.J.; Greenough, M.A.; Volitakis, I.; Adlard, P.A.; Cherny, R.A.; et al. The Alzheimer's therapeutic PBT2 promotes amyloid- β degradation and GSK3 phosphorylation via a metal chaperone activity. *J. Neurochem.* **2011**, *119*, 220–230. [[CrossRef](#)]
39. Biancalana, M.; Koide, S. Molecular mechanism of Thioflavin-T binding to amyloid fibrils. *Biochim. Biophys. Acta.* **2010**, *1804*, 1405–1412. [[CrossRef](#)]
40. Crescenzi, O.; Tomaselli, S.; Guerrini, R.; Salvadori, S.; D'Ursi, A.M.; Temussi, P.A.; Picone, D. Solution structure of the Alzheimer amyloid β -peptide (1–42) in an apolar microenvironment. Similarity with a virus fusion domain. *Eur. J. Biochem.* **2002**, *269*, 5642–5648. [[CrossRef](#)]

41. Du, H.; Liu, X.; Xie, J.; Ma, F. Novel Deoxyvasicinone–Donepezil Hybrids as Potential Multitarget Drug Candidates for Alzheimer’s Disease. *ACS Chem. Neurosci.* **2019**, *10*, 2397–2407. [[CrossRef](#)] [[PubMed](#)]
42. Lu, C.; Guo, Y.; Yan, J.; Luo, Z.; Luo, H.-B.; Yan, M.; Huang, L.; Li, X. Design, Synthesis, and Evaluation of Multitarget-Directed Resveratrol Derivatives for the Treatment of Alzheimer’s Disease. *J. Med. Chem.* **2013**, *56*, 5843–5859. [[CrossRef](#)] [[PubMed](#)]

Sample Availability: Samples of the compounds are available from the authors.



© 2020 by the authors. Licensee MDPI, Basel, Switzerland. This article is an open access article distributed under the terms and conditions of the Creative Commons Attribution (CC BY) license (<http://creativecommons.org/licenses/by/4.0/>).